Flow pattern in the vicinity of self-propelling hot Janus particles

Thomas Bickel, Arghya Majee, Alois Würger

Flow pattern in the vicinity of self-propelling hot Janus particles

Thomas Bickel,[1] Arghya Majee,[1, 2] and Alois Würger[1, 3]

[1]*LOMA, Université de Bordeaux & CNRS, 351 cours de la Libération, 33405 Talence, France*
[2]*Max-Planck-Institut für Intelligente Systeme, Heisenbergstraße 3, 70569 Stuttgart, Germany*
[3]*ZHS, Universität Leipzig, Burgstraße 21, 04103 Leipzig, Germany*

We study the temperature field and the resulting flow pattern in the vicinity of a heated metal-capped Janus particle. If its thickness exceeds about ten nanometers, the cap forms an isotherm and the flow pattern comprises a quadrupolar term that decays with the square of the inverse distance $\sim r^{-2}$. For much thinner caps the velocity varies as $\sim r^{-3}$. These findings could be relevant for collective effects in dense suspensions and for the circular tracer motion observed recently in the vicinity of a tethered Janus particle.

I. INTRODUCTION

The design of artificial micro- and nano-swimmers that propel themselves in a viscous fluid is a key issue in nanotechnology [1]. In the realm of biology, autonomous motion of microorganisms is ubiquitous and relies on surface waves or periodic body deformations [2]. Several swimming devices inspired by living systems have been built recently [3, 4], although their actuation mechanism requires external forces or torques. An alternative way toward self-propulsion is achieved using colloidal particles with non-uniform surface properties [5]. This class of rigid swimmers relies on phoretic transport, *i.e.* the force-free motion driven by the gradient of an external field [6]. In the case of self-phoresis, however, asymmetric particles are able to generate their own gradient within an otherwise homogeneous medium and thus to convert the available energy into mechanical work [7, 8].

The simplest realization of autonomous swimmers is obtained with Janus particles, which are colloidal objects with two sides differing in their physical or chemical properties [9]. For example, a bimetallic particle in a peroxide solution generates a electrochemical gradient which in turn gives rise to a flow in the surrounding fluid and thus causes self-propulsion [10]. At short times this results in linear motion, whereas at longer times the random reorientations lead to enhanced diffusion [11, 12]. Similar findings have been reported for photophoresis of hot Janus particles, which move in their own temperature gradient with an effective diffusion coefficient that increases linearly with the heating power [13–15].

Heating of metal capped Janus particles provides a versatile means of actuation which, in particular, can be switched on and off almost instantaneously. Heat absorption of the metal cap is achieved upon illumination by a defocused laser beam [13–16] or when subject to an ac magnetic field [17]. The metal patch absorbs the energy and converts it into heat; asymmetric heat release then drives the colloid via a mechanism of thermophoresis [6].

In this article we address the temperature profile and the fluid velocity in the vicinity of a hot Janus particle. In view of its large thermal conductivity we treat the metal cap as an isotherm and, as a consequence, obtain a class of hydrodynamic multipoles that are absent when neglecting heat conduction in the cap. These aditionall terms result in a flow pattern which is strongly asymmetric with respect to the particle midplane, and could affect the hydrodynamic coupling between neighboring swimmers or with a bounding wall [18–20]. On the other hand, a fixed Janus particle is expected to act as a micropump. Visualization of the local convective flow by particle tracking velocimetry indeed revealed vortices close to a Janus particle tethered on a glass support [13]. The description of tracers trajectories thus requires a detailed knowledge of both the temperature and the velocity fields around a Janus particle.
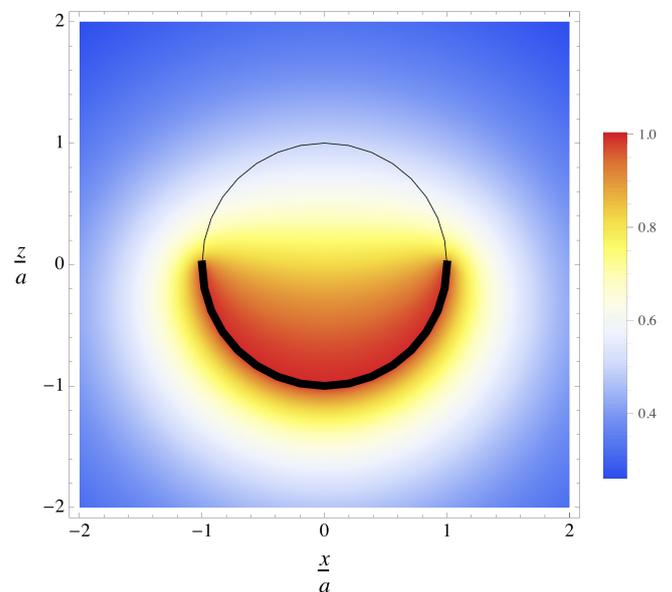

FIG. 1: (Color online) Map of the reduced temperature $(T-T_0)/\Delta T$ in the (xOz) plane, inside and outside the metal-coated colloid. The thick line represents the metal layer, where the temperature is at its maximum. It then decreases monotonically to the bulk value.

II. TEMPERATURE FIELD

In a first step we derive the temperature profile from Fourier's law

$$\kappa \nabla^2 T = q(\mathbf{r}) \;, \tag{1}$$

where q is the power absorbed by the metal cap, and κ the thermal conductivity of both the particle and the surrounding fluid (taken to be the same for simplicity). The cap conductivity κ_c is usually much higher than κ; if their ratio is larger than the ratio of particle radius and cap thickness, $\kappa_c/\kappa > a/d$, the cap forms an isotherm. Since this condition is satisfied for a 50 nm gold cap on micron-size silica or polystyrene beads, we assume in the following a constant cap temperature $T_0 + \Delta T$. Typical values for the excess temperature ΔT with respect to the bulk are of the order of a few Kelvins.

Because of the mixed boundary conditions, constant temperature on the metal cap and heat flux continuity on the upper hemisphere, there is no straightforward solution of Eq. (1). As shown in the Appendix, the global constraint on the isotherm can be implemented by a method based on auxiliary functions. Here we merely quote the temperature profile in the liquid phase ($r > a$)

$$T(r,\theta) = T_0 + \frac{\Delta T}{\pi} \sum_{n=0}^{\infty} t_n P_n(c) \left(\frac{a}{r}\right)^{n+1} \;, \tag{2}$$

with $c = \cos\theta$ and the Legendre polynomial P_n. The coefficients t_n are given by

$$t_{2k} = -t_{2k+1} = \frac{(-1)^k}{2k+1} \;, \tag{3}$$

except for the first one that reads $t_0 = 1 + \pi/2$. A similar expression with the same coefficients is found inside the particle ($r < a$), albeit with $(r/a)^n$ instead of $(a/r)^{n+1}$. Identifying the power $\mathcal{P}$ absorbed by the metal cap with the total outward heat flow, one readily establishes the relation with the excess temperature: $\mathcal{P} = (2\pi+4)\kappa a\Delta T$. The map of the temperature field is shown in Fig. 1. The role of the isotherm assumption is illustrated by comparing with the case of a very thin cap where $\kappa_c/\kappa < a/d$. Then the heat conductivity of the metal structure can be neglected, and we show in the Appendix that the even coefficients of the temperature profile vanish: $t_{2k} = 0$ [13].

III. BOUNDARY VELOCITY

The temperature gradient modifies the particle-solvent interactions in a boundary layer of thickness ℓ. For electric-double layer forces ℓ is given by the Debye length, and for depletion forces by the gyration radius of the polymers. In both cases ℓ is much smaller than the radius a of micron size colloidal particles, such that the flow pattern in the liquid can be evaluated in boundary layer approximation [6, 21, 22]. The excess enthalpy density h
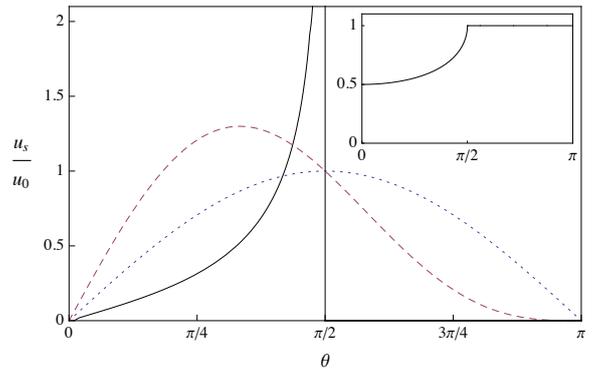

FIG. 2: (Color online) Quasi-slip velocity $u_s(\theta)$ as a function of the polar angle θ. For comparison, we plot the infinite series (4) (solid line), the dipolar approximation (series truncated at $n = 1$, dotted line) and the quadrupolar approximation (series truncated at $n = 2$, dashed line). Inset: surface temperature $[T(a,\theta) - T_0]/\Delta T$ as a function of θ.

results in a quasi-slip velocity of the liquid with respect to the particle [23].

The boundary velocity is proportional to the temperature gradient parallel to the surface of the particle $u_s = -(\ell^2\bar{h}/\eta T_0)\nabla T_{\parallel}$, where η is the viscosity and $\bar{h}$ the characteristic value of the excess enthalpy. With Eq. (2) one has

$$u_s(\theta) = u_0 \sum_{n=1}^{\infty} t_n \frac{dP_n(c)}{d\theta} \;, \tag{4}$$

where the prefactor u_0 gives the velocity scale,

$$u_0 = -\frac{\ell^2\bar{h}}{\pi\eta a}\frac{\Delta T}{T_0} \;. \tag{5}$$

The first term in Eq. (4) corresponds to the dipolar approximation: $u_s(\theta) = u_0 \sin\theta$ [6]. Keeping the first two terms of the series, the surface velocity is that of a "squirmer" with positive stresslet $\beta = 2/3$ [19, 24].

For positive slip velocity u_0, i.e., negative enthalpy $\bar{h}$, the liquid flows toward the warmer side of the Janus particle. Note that u_s is largest on the upper half-sphere close to mid-plane; it vanishes on the lower half-sphere because of the constant temperature of the metal cap – see Fig. 2. The expression $\ell^2\bar{h}$ has the dimension of a force, and has been evaluated for several thermophoretic mechanisms. Ruckenstein pointed out the positive slip velocity ($u_0 > 0$) due to the enthalpy of the electric double layer, $\ell^2\bar{h} = -\frac{1}{2}\varepsilon\zeta^2$ [25], with the surface potential ζ and the solvent permittivity ε. In many instances, however, the slip velocity is dominated by the thermoelectric effect $\ell^2\bar{h} = \frac{3}{2}\varepsilon\zeta ST_0$, where the electrolyte Seebeck coefficient S may take either sign [26–28]. Upon adding polymer to the solution, thermal depletion forces result in $u_0 < 0$ [29]. For a micro-size particle with $\Delta T = 1$ K, the slip velocity is a few microns per second.

IV. BULK VELOCITY FIELD

The quasi-slip velocity on the surface of the particle induces a flow in the surrounding liquid. The general axisymmetric solution $\mathbf{v} = v_r\mathbf{e}_r + v_\theta\mathbf{e}_\theta$ of the Stokes' equation has been known for a long time [24, 30]. Here we give the series expansion of Ref. [31], where the radial and tangential components are given by

$$v_r = u_0 \sum_{n=1}^{\infty} \frac{a^n}{r^n}\left(p_n + q_{n+2}\frac{a^2}{r^2}\right) P_n(c) \ , \quad (6a)$$

$$v_\theta = u_0 s \sum_{n=1}^{\infty} \frac{a^n}{r^n}\left(p_n\frac{n-2}{n(n+1)} + \frac{q_{n+2}}{n+1}\frac{a^2}{r^2}\right) P_n'(c) \ , \quad (6b)$$

with $P_n' = dP_n/dc$ and $s = \sin\theta$. The coefficients p_n describe the inhomogeneous solutions of Stokes' equation with finite pressure, whereas the q_n's are related to the zero-pressure homogeneous solutions. The coefficients are set by the boundary conditions at the surface of the particle. First, the far field $\mathbf{v}$ has to match the sum of the particle velocity $u_p\mathbf{e}_z$ and the quasi-slip velocity

$$\mathbf{v}|_{r=a} = u_p\mathbf{e}_z + u_s\mathbf{e}_\theta \ . \quad (7)$$

The second condition is a global constraint and involves the total force $F_z = -4\pi\eta u_0 a p_1$. In the following we evaluate the coefficients for a particle that is either freely moving of fixed at a given position.

V. MOVING PARTICLE

First we consider a free Janus particle that self-propels due its own temperature gradient. Since there is no external force, the global constraint imposes the well-known condition $p_1 = 0$ [6]. Yet, the no-force condition does not affect the inhomogeneous coefficients of higher order. Noting $\mathbf{e}_z = c\,\mathbf{e}_r - s\,\mathbf{e}_\theta$, one obtains the radial and tangential projections of Eq. (7), $v_r = cu_p$ and $v_\theta = -su_p + u_s$. Inserting Eqs. (6a) and (6b), one readily gets for $n = 1$

$$p_1 = 0 \ , \quad \text{and} \quad q_3 = -\frac{2}{3}t_1 = \frac{2}{3} \ , \quad (8)$$

and for higher orders

$$p_n = -q_{n+2} = \frac{n(n+1)}{2}t_n \qquad (n \geq 2) \ . \quad (9)$$

The particle velocity is then in opposite direction to the quasi-slip and is equal to two thirds of its amplitude

$$u_p = q_3 u_0 = \frac{2}{3}u_0 \ . \quad (10)$$

This implies that self-propulsion is driven by the dipolar term q_3 only; higher Fourier coefficients of the temperature gradient, t_n with $n > 1$, do not contribute to the particle velocity.
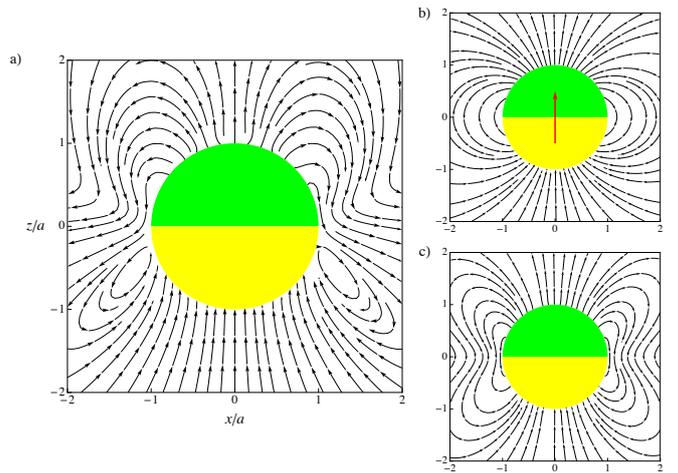

FIG. 3: (Color online) Flow streamlines around a moving Janus particle in the laboratory frame. a) The cap forms an isotherm with t_k as in (3). b) Dipolar approximation with t_1 only. c) Thin-cap limit, with $t_{2k} = 0$.

We emphasize two major differences with respect to the thin-cap limit, where $t_{2n} = 0$ and the dipolar approximation where t_1 is the only non-zero coefficient. First, the temperature coefficient t_2 results in a radial velocity contribution that decays with the square of the inverse distance and shows quadrupole characteristics. In the thin-cap and dipolar approximations the velocity decays as r^{-3}. Second, Fig. 3a) shows that the rotational patterns of the stream lines are located close to the metal cap; for comparison, we also plot the dipolar flow field with the only coefficient q_3 and the thin-cap limit with $t_{2k} = 0$ [13]. The corresponding streamlines in Fig. 3b) and c) are symmetric with respect to midplane.

In Fig. 4 we plot both v_r and v_θ as a function of θ at a distance $r = 1.5a$ from the center of the particle; we compare the whole series with the dipolar approximation ($n = 1$ only), and the quadrupolar approximation ($n = 1, 2$). The dipolar terms are simply given by sine and cosine functions. The quadrupolar correction is by no means small or insignificant; for example, v_r changes sign at small θ, and v_θ at angles close to π. Retaining the higher-order corrections again changes the flow pattern drastically. As the most striking feature, note the large positive derivative $dv_r/d\theta$ close to midplane; together with the positive value of the tangential component v_θ this implies the existence of vortices at the edge of the metal cap.

VI. IMMOBILE PARTICLE

Now we turn to the situation where the Janus particle is fixed at a given position. This requires a finite external force that counteracts the self-propelling surface stress in the boundary layer. The particle velocity is then zero, $u_p = 0$, so that the quasislip velocity matches to the
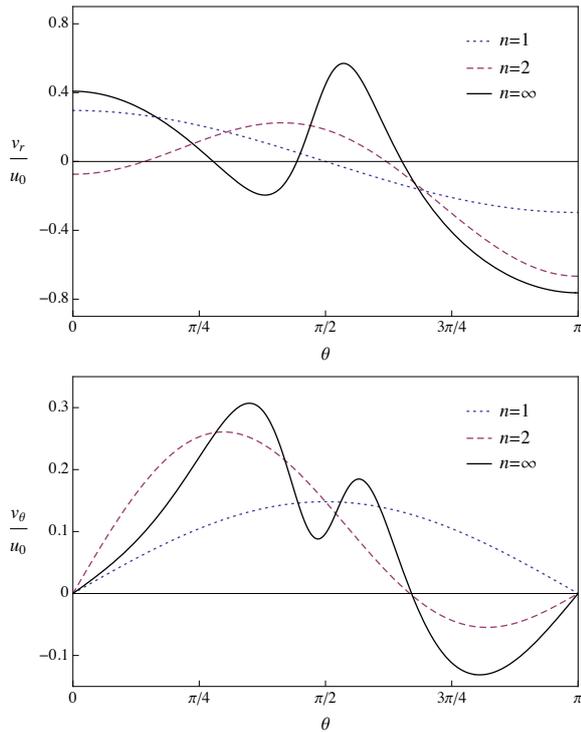
FIG. 4: (Color online) Radial and tangential components of the velocity of a moving particle at distance $r = 1.5a$ from its center. The plots correspond to the series (6a) and (6b) truncated at $n = 1$ (dipolar approximation, dotted lines), truncated at $n = 2$ (quadrupolar approximation, dashed lines), and to the infinite series (solid lines).

FIG. 5: (Color online) Map of the tracer velocity $\mathbf{u}_t$ for different values of the parameter ξ.

tangential component of the far-field $u_\theta = v_\theta$, whereas the radial component vanishes $v_r = 0$. One obtains the coefficients for the flow pattern

$$p_n = -q_{n+2} = \frac{n(n+1)}{2} t_n \qquad (n \geq 1) . \qquad (11)$$

With the coefficient $p_1 = -1$ one finds the external force $F_z = 4\pi\eta a u_0$. It is required to immobilize the particle which otherwise would move at a velocity $u_p = \frac{2}{3} u_0$, and thus corresponds to the well-known Stokes drag $6\pi\eta a u_p$.

In Fig. 5a) we plot the flow pattern $\mathbf{v}(r, \theta)$. Contrary to that of the moving particle, there are no vortices close to the particle; the liquid flows smoothly around the immobile particle. Comparison of the coefficients shows that this difference is only due to the lowest-order coefficients $p_1 = -1$ and $q_3 = 1$; in other words, the large long-range contribution p_1 hides the vortices that accompany a moving particle but are invisible in the case where the particle is fixed.

VII. MOTION OF A TRACER PARTICLE

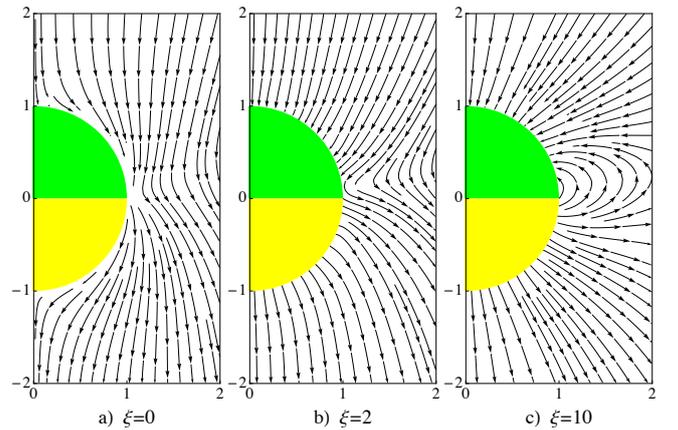Finally, we consider a small tracer in the neighborhood of a fixed Janus particle. Its velocity $\mathbf{u}_t$ is given by the sum of the convective flow and of thermophoretic drift in the temperature gradient of the Janus particle

$$\mathbf{u}_t = \mathbf{v}(\mathbf{r}) - D_T \nabla T , \qquad (12)$$

with $\mathbf{v}(\mathbf{r})$ given by Eqs. (6) and (11). The mobility coefficient D_T is expressed by the enthalpy density and thickness of the boundary layer of the tracer [22]. The vector fields $\mathbf{v}$ and ∇T have different characteristics: at large distance, the first is isotropic and the second one of quadrupolar symmetry; close to the particle higher order terms lead to an even more intricate variation. The relative importance of the two terms in (12) is expressed by the mobility ratio of tracer and Janus particle, $\xi = D_T / \hat{D}_T$, which depends on their surface properties. Either term in Eq. (12) may be dominant, and they may even carry opposite sign.

In Fig. 5 we plot the tracer velocity $\mathbf{u}_t$ for $\xi = 0$, 2 and 10. As the most striking feature, the tracer is pushed toward the colder half of the Janus particle from above but is strongly repelled from the warmer side. For $\xi = 0$ (no thermophoresis), the tracer first flows toward the Janus particle, then creeps slowly toward the metal cap, and finally is repelled from it. For intermediate value $\xi = 2$, transport alongside the surface has ceased and tracer particles either accumulate at the upper side or are pushed away from the lower side. For the larger value $\xi = 10$, the flow pattern shows additional vortices close to the midplane of the Janus particle, so that tracers are brought back to the colder side.

Experimentally, flow circulation around a heated Janus particle tethered to a glass surface has been reported recently [13]. Tracking of fluorescent particles moreover revealed that the concentration of tracers is higher on the non-coated side and lower on the coated side. It is thus likely that the observed flow pattern results from the competition between convection and thermophoresis, as expressed by Eq. (12).

VIII. CONCLUSION

In summary, we have characterized the flow around a heated Janus colloid. The discontinuity of surface properties has a major impact on the fluid velocity field not only in the vicinity of the particle but also in the bulk. In particular, we have shown that the dipolar approximation which is usually considered for simplicity is only a poor approximation of the full series. Taking into account higher order terms leads to a complex flow field that can be relevant at finite concentration, where collective effects come into play [20, 32].

Appendix A: Temperature profile around a metal-capped colloid

In this appendix, we solve the heat equation around a spherical colloid with inhomogeneous surface properties. More precisely, we consider a bead of radius a and thermal conductivity κ_{in} in a fluid of thermal conductivity κ_{out}. For the sake of convenience, we assume here that the metal-capped hemisphere is the upper one, whereas the opposite assumption was made in the text. Still, one just has to multiply the coefficients by a factor $(-1)^n$ to switch from one configuration to another.

We assume that the sphere is centered at $r = 0$. Inside and outside the particle, the temperature is solution of the stationary heat equation

$$\nabla^2 T = 0 , \quad (A1)$$

whose general axisymmetric solution reads

$$T_{in}(r, \theta) = T_0 + \sum_{n=0}^{\infty} \alpha_n \left(\frac{r}{a}\right)^n P_n(\cos\theta) , \quad (A2a)$$

$$T_{out}(r, \theta) = T_0 + \sum_{n=0}^{\infty} \alpha_n \left(\frac{a}{r}\right)^{n+1} P_n(\cos\theta) , \quad (A2b)$$

with P_n the Legendre polynomials. Note that we have enforced the continuity condition $T_{in}(a, \theta) = T_{out}(a, \theta)$. We have also assumed that the temperature remains finite far away from the particle: $T(r \gg a, \theta) = T_0$.

The coefficients $\{\alpha_n\}$ are obtained from the appropriate boundary conditions. Heat flux continuity on the lower part of the sphere reads

$$\kappa_{in}\partial_r T_{in} = \kappa_{out}\partial_r T_{out} . \quad (A3)$$

In most practical cases heat conductivities of the solvent and of the colloid are very close to one another, so that we can set $\kappa_{in} = \kappa_{out} = \kappa$.

The situation on the capped hemisphere is more elaborate. The upper part of the sphere is covered with a thin metal layer of thickness d and thermal conductivity κ_c. Inside the metal layer, one would have to solve the heat equation with a constant source term Q accounting for heat absorption; heat flux continuity should then be enforced at the boundaries. The approach that we develop below is less involved and takes advantage of the separation of length scales. Indeed, the thickness of the metal layer ($d \simeq 50$ nm) is usually much smaller than the size of the particle ($a \simeq 1$ μm). The metal cap is then treated as a boundary condition, and two limiting situations will be considered:

- $\kappa_c d \ll \kappa a$: in the thin cap limit, the thermal conductivity of the cap is irrelevant and the heat flux condition reads

$$-\kappa_{out}\partial_r T_{out}(a, \theta) + \kappa_{in}\partial_r T_{in}(a, \theta) = q , \quad (A4)$$

with $q = Qe$. This situation was considered for instance by Jiang et $al.$ [13] and is summarized in Sec. A 1.

- $\kappa d \gg \kappa_p a$: in the thick cap limit, heat conductivity is so large that the cap is at constant temperature

$$T(a, \theta) = T_0 + \Delta T , \quad (A5)$$

where ΔT can be related to Q by evaluating the total heat flux. This limit is discussed in Sec. A 2.

1. Thin cap limit

In this limit, it is assumed that the continuity of flux at the particle surface ($r = a$) including laser heat absorption reads

$$-\kappa_{out}\partial_r T_{out} + \kappa_{in}\partial_r T_{in} = q(\theta) , \quad (A6)$$

with $q(\theta) = q$ for $0 \leq \theta < \pi/2$, and $q(\theta) = 0$ for $\pi/2 < \theta \leq \pi$. To solve the problem, we expand $q(\theta)$ as a Legendre-Fourier series

$$q(\theta) = \sum_{n=0}^{\infty} q_n P_n(\cos\theta) , \quad (A7)$$

the coefficients $\{q_n\}$ being given by

$$q_n = \frac{2n+1}{2} \int_0^{\pi} q(\theta) P_n(\cos\theta) \sin\theta \mathrm{d}\theta$$

$$= \frac{q}{2}(2n+1) \int_0^1 P_n(x) \mathrm{d}x . \quad (A8)$$

The integral $I_n = \int_0^1 P_n(x)\mathrm{d}x$ is readily evaluated [33]: $I_0 = 1$, $I_{2k} = 0$ for $k \geq 1$, and

$$I_{2k+1} = \frac{(-1)^k (2k)!}{2^{2k+1} k!(k+1)!} . \quad (A9)$$

From the general solution (A2), the boundary condition (A6) can then be expressed as

$$\sum_{n=0}^{\infty} [(n+1)\kappa_{out} + n\kappa_{in}] \alpha_n P_n(\cos\theta) = aq(\theta) , \quad (A10)$$

so that we get

$$\alpha_n = \frac{aq_n}{(n+1)\kappa_{out} + n\kappa_{in}} \ . \qquad (A11)$$

This completely solves the problem. If we set $\kappa_{in} = \kappa_{out} = \kappa$, the coeficients $\{\alpha_n\}$ are finally given by

$$\alpha_0 = \frac{aq}{2\kappa} \ , \qquad (A12a)$$

$$\alpha_{2k} = 0 \quad \text{for} \quad k \geq 1 \ , \qquad (A12b)$$

$$\alpha_{2k+1} = \alpha_0 \frac{(-1)^k (2k)!}{2^{2k+1} k!(k+1)!} \ . \qquad (A12c)$$

2. Thick cap limit

We now assume that the capped hemisphere is held at constant temperature, whereas heat flux continuity is imposed on the lower hemisphere. To solve this mixed boundary value problem, we follow closely the derivation of Ref. [34]. For the sake of simplicity we shall assume that $\kappa_{in} = \kappa_{out}$. The boundary conditions (A3) and (A5) then lead to the following relations

$$\sum_{n=0}^{\infty} \alpha_n P_n(\cos\theta) = \Delta T \ , \quad 0 \leq \theta < \pi/2 \ , \qquad (A13a)$$

$$\sum_{n=0}^{\infty} (2n+1)\alpha_n P_n(\cos\theta) = 0 \ , \quad \pi/2 < \theta \leq \pi \ . \quad (A13b)$$

To solve the problem, it is useful to introduce two auxiliary functions $g(\theta)$ and $h(\theta)$ according to

$$g(\theta) = -\frac{1}{\sin\theta} \frac{d}{d\theta} \int_{\theta}^{\pi/2} \frac{h(u)}{\sqrt{\cos\theta - \cos u}} du \ , \qquad (A14)$$

for $0 \leq \theta < \pi/2$, and $g(\theta) = 0$ for $\pi/2 < \theta \leq \pi$. We can therefore write

$$\sum_{n=0}^{\infty} (2n+1)\alpha_n P_n(\cos\theta) = g(\theta) \ , \quad \forall \theta \in [0, \pi] \ . \quad (A15)$$

Note that Eq. (A15) actually defines the Fourier coefficients of $g(\theta)$.

The strategy is then the following : starting from the definition of $g(\theta)$, we derive a relation between the coefficients $\{\alpha_n\}$ and the (yet unknown) function $h(\theta)$. Using the boundary condition Eq. (A13a), we next establish an explicit expression for the function $h(\theta)$ from which we obtain the coefficients $\{\alpha_n\}$.

According to the orthogonality condition of Legendre polynomials, the coefficients α_n can be expressed as

$$\alpha_n = \frac{1}{2} \int_0^{\pi} d\theta \sin\theta P_n(\cos\theta) g(\theta)$$

$$= \frac{1}{2} \int_0^{\pi/2} du \frac{h(u)}{\sin u} \times I'(u) \ ,$$

where the integral $I(u)$ is defined as [34]

$$I(u) = \int_0^u d\theta P_n(\cos\theta) \frac{\sin\theta}{\sqrt{\cos\theta - \cos u}} \ .$$

To evaluate $I(u)$, we use the representation of Legendre polynomials as Mehler's integrals [33]

$$P_n(\cos\theta) = \frac{\sqrt{2}}{\pi} \int_0^{\theta} dx \frac{\cos(n+1/2)x}{\sqrt{\cos x - \cos\theta}} \ .$$

The integral $I(u)$ then reads

$$I(u) = \sqrt{2} \int_0^u dx \cos(n+1/2)x = \frac{\sqrt{2}}{n+1/2} \sin(n+1/2)u \ ,$$

so that we get

$$\alpha_n = \frac{1}{\sqrt{2}} \int_0^{\pi/2} du \, h(u) \frac{\cos(n+1/2)u}{\sin u} \ . \qquad (A16)$$

We still need to get an explicit expression for the (yet unknown) function $h(\theta)$. To this aim, we substitute the expression (A16) for α_n into Eq. (A13a). Interchanging the order of integration and summation we get for $0 \leq \theta < \pi/2$

$$\frac{1}{\sqrt{2}} \int_0^{\pi/2} du \frac{h(u)}{\sin u} \sum_{n=0}^{\infty} P_n(\cos\theta) \cos(n+1/2)u = \Delta T \ .$$

As a matter of fact, the latter series is given by [33]

$$\sum_{n=0}^{\infty} P_n(\cos\theta) \cos(n+1/2)u = \frac{1}{\sqrt{2}} \frac{H(\theta - u)}{\sqrt{\cos u - \cos\theta}} \ ,$$

for $0 < u, \theta < \pi$, with H the Heaviside function. We then obtain

$$\frac{1}{2} \int_0^{\pi/2} du \frac{h(u)}{\sin u} \frac{H(\theta - u)}{\sqrt{\cos u - \cos\theta}} = \Delta T \ ,$$

for $0 \leq \theta < \pi/2$. This equation can readily be inverted in order to get an explicit expression for the function $h(u)$

$$h(u) = \frac{2}{\pi} \Delta T \sin u \frac{d}{du} \left(\int_0^u d\theta \frac{\sin\theta}{\sqrt{\cos\theta - \cos u}} \right)$$

$$= \frac{2\sqrt{2}}{\pi} \Delta T \sin u \cos u/2 \ . \qquad (A17)$$

Eqs. (A16) and (A17) give the solution of the problem. We finally obtain

$$\alpha_n = \frac{2}{\pi} \Delta T \int_0^{\pi/2} du \cos u/2 \cos(n+1/2)u \ ,$$

so that

$$\alpha_0 = \left(\frac{1}{2} + \frac{1}{\pi} \right) \Delta T \ , \qquad (A18a)$$

$$\alpha_{2k} = \alpha_{2k+1} = \frac{(-1)^k}{2k+1} \frac{\Delta T}{\pi} \ . \qquad (A18b)$$

[1] S.J. Ebbens and J.R. Howse, Soft Matter **6**, 726–738 (2010)

[2] E. Lauga and T.R. Powers, Rep. Prog. Phys. **72**, 096601 (2009)

[3] R. Dreyfus, J. Baudry, M.L. Roper, M. Fermigier, H.A. Stone, and J. Bibette, Nature **437**, 862 (2005)

[4] A. Gosh and P. Fisher, Nano Lett. **9**, 2243 (2009)

[5] R. Golestanian, T.B. Liverpool, and A. Ajdari, Phys. Rev. Lett. **94**, 220801 (2005)

[6] J.O. Anderson, Ann. Rev. Fluid Mech. **21**, 61 (1989)

[7] R. Golestanian, T.B. Liverpool, and A. Ajdari, New J. Phys. **9**, 126 (2007)

[8] F. Julicher, J. Prost, Eur. Phys. J. E **29**, 27 (2009)

[9] A. Walther and A.H.E. Müller, Soft Matter **4**, 663–668 (2008)

[10] W. F. Paxton, A. Sen, and T. E. Mallouk, Chem. Eur. J. **11**, 6462 (2005).

[11] J.R. Howse, R.A.L. Jones, A.J. Ryan, T. Gough, R. Vafabakhsh, and R. Golestanian, Phys. Rev. Lett. **99**, 048102 (2007)

[12] G. Dunderdale, S. Ebbens, P. Fairclough, and J. Howse, Langmuir **28**, 10997 (2012)

[13] H.-R. Jiang, N. Yoshinaga, M. Sano, Phys. Rev. Lett. **105**, 268302 (2010)

[14] G. Volpe, I. Buttinoni, D. Vogt, H.-J. Kümmerer, and C. Bechinger, Soft Matter **7**, 8810 (2011)

[15] I. Buttinoni, G. Volpe, F. Kümmel, G. Volpe, C. Bechinger, J. Phys.: Cond. Mat. **24**, 284129 (2012)

[16] B. Qian, D. Montiel, A. Bregulla, F. Cichos, H. Yang, Chem. Sci. **4**, 1420 (2013)

[17] L. Baraban, R. Streubel, D. Makarov, L., D. Kar-naushenko, O.G. Schmidt, G. Cuniberti, ACS Nano **7**, 1360 (2013)

[18] T. Ishikawa, M. Simmonds, T. Pedley, J. Fluid Mech. **568**, 119 (2006)

[19] I. Llopis and I. Pagonabarraga, J. Non-Newtonian Fluid Mech. **165**, 946 (2010).

[20] R. Golestanian, Phys. Rev. Lett. **108**, 038303 (2012)

[21] S. Fayolle, T. Bickel, A. Würger, Phys. Rev. E **77**, 042404 (2008)

[22] A. Würger, Rep. Prog. Phys., **73**, 126601 (2010)

[23] B. Derjaguin, N. Churaev, V. Muller, *Surface Forces* (Plenum, New York, 1987)

[24] J.R. Blake, J. Fluid Mech. **46**, 199 (1971)

[25] E. Ruckenstein, J. Coll. Interf. Sci., **83**, 77 (1981)

[26] S.A. Putnam, D.G. Cahill., Langmuir **21**, 5317 (2005)

[27] A. Würger, Phys. Rev. Lett., **101**, 108302 (2008)

[28] D. Vigolo, S. Buzzaccaro and R. Piazza, Langmuir, **26**, 7792 (2010)

[29] H.-R. Jiang, H. Wada, N. Yoshinaga and M. Sano, Phys. Rev. Lett., **102**, 208301 (2009)

[30] H. Brenner, Chem. Eng. Sci. **16**, 242 (1961)

[31] J. Morthomas, A. Würger, Phys. Rev. E **81**, 051405 (2010)

[32] I. Theurkauff, C. Cottin-Bizonne, J. Palacci, C. Ybert, L. Bocquet, Phys. Rev. Lett. **108**, 268303 (2012)

[33] I.S. Gradshteyn and I.M. Ryzhik, "Table of integrals, series, and products", 7th edition (Academic Press, San Diego, 2007)

[34] I.N. Sneddon, "Mixed boundary value problems in potential theory" (Wiley, NY, 1966)